European Journal of Mechanics / A Solids 100 (2023) 104991

Contents lists available at ScienceDirect

European Journal of Mechanics / A Solids

journal homepage: www.elsevier.com/locate/ejmsol

Accelerated high-cycle phase field fatigue predictions

Philip K. Kristensen [a], Alireza Golahmar [a,b], Emilio Martínez-Pañeda [b], Christian F. Niordson [a,*]

[a] Department of Civil and Mechanical Engineering, Technical University of Denmark, DK-2800 Kgs. Lyngby, Denmark
[b] Department of Civil and Environmental Engineering, Imperial College London, London SW7 2AZ, UK

ARTICLE INFO

Keywords:
Fatigue
Phase field fracture
Fracture mechanics
Finite element analysis

ABSTRACT

Phase field fracture models have seen widespread application in the last decade. Among these applications, its use to model the evolution of fatigue cracks has attracted particular interest, as fatigue damage behaviour can be predicted for arbitrary loading histories, dimensions and complexity of the cracking phenomena at play. However, while cycle-by-cycle calculations are remarkably flexible, they are also computationally expensive, hindering the applicability of phase field fatigue models for technologically-relevant problems. In this work, a computational framework for accelerating phase field fatigue calculations is presented. Two novel acceleration strategies are proposed, which can be used in tandem and together with other existing acceleration schemes from the literature. The computational performance of the proposed methods is documented through a series of 2D and 3D boundary value problems, highlighting the robustness and efficiency of the framework even in complex fatigue problems. The observed reduction in computation time using both of the proposed methods in tandem is shown to reach a speed-up factor of 32, with a scaling trend enabling even greater reductions in problems with more load cycles.

1. Introduction

The phase field fracture model has received substantial attention in the last decade — and for good reason. The original model, proposed by Bourdin et al. (2000) as a regularization of the variational fracture formulation by Francfort and Marigo (1998), is flexible and simple to implement numerically. It can readily capture complex cracking phenomena such as crack branching (Borden et al., 2012), coalescence (Kristensen et al., 2020b), complex crack trajectories (Hirshikesh et al., 2019) and crack nucleation from non-sharp defects (Tanné et al., 2018). Moreover, it can naturally capture the crack size effect (Tanné et al., 2018; Kristensen et al., 2021) and be readily extended to accommodate specific failure surfaces (Navidtehrani et al., 2022; Lorenzis and Maurini, 2022). The model has proven to be extremely versatile and thus has been used in a vast number of applications, both within complex fracture problems such as cohesive fracture (Wu, 2017; Feng and Li, 2022), micromechanical damage (Guillén-Hernández et al., 2020; Tan and Martínez-Pañeda, 2021), and ductile fracture (Aldakheel et al., 2018; Alessi et al., 2018), but also in multi-physics applications ranging from thermal shocks (Bourdin et al., 2014) and moisture effects (Ye and Zhang, 2022) to hydrogen embrittlement (Martínez-Pañeda et al., 2018; Duda et al., 2018; Anand et al., 2019; Kristensen et al., 2020a) and Lithium-ion battery degradation (Klinsmann et al., 2016; Boyce et al., 2022; Ai et al., 2022).

Among the many problems attracting phase field developments, fatigue is arguably one of the most important ones, from both scientific and technological perspectives. Using phase field as a framework for fatigue models is an attractive prospect (Alessi and Ulloa, 2023), as fatigue remains a longstanding challenge in solid mechanics and a sufficiently flexible phase field fatigue model could readily encompass the aforementioned phase field models and applications. An example of such a flexible framework is found in the work by Carrara et al. (2020), where a history variable is introduced to introduce a dependence of the fracture energy on the loading history of the material. The model naturally recovers the Paris Law and S–N curve behaviour and has proven an attractive platform from which to develop phase field fatigue models for various applications (Loew et al., 2020; Golahmar et al., 2022; Simoes and Martínez-Pañeda, 2021; Simoes et al., 2022). Aside from Carrara et al. (2020), there have been several other notable works, both of a cycle-by-cycle nature (Seiler et al., 2020; Mesgarnejad et al., 2019; Song et al., 2022) and more practical approaches, which take the Paris behaviour as an input (Lo et al., 2019).

Two known drawbacks associated with phase field fracture are the computational cost associated with the need for a sufficiently fine mesh to resolve the phase field length scale (Kristensen et al., 2021), and the inefficiency of the solution due to the non-convexity of the balance equations (Gerasimov and De Lorenzis, 2016). Significant efforts have been extended towards remedying both issues.

* Corresponding author.
E-mail address: cfni@dtu.dk (C.F. Niordson).

https://doi.org/10.1016/j.euromechsol.2023.104991
Received 18 January 2023; Received in revised form 1 April 2023; Accepted 2 April 2023
Available online 4 April 2023

Strategies to ease meshing requirements include adaptive mesh refinement (Heister et al., 2015; Klinsmann et al., 2015; Freddi and Mingazzi, 2022, 2023), specialized element formulations (Olesch et al., 2021) and the use of a combined finite element-finite volume approach (Sargado et al., 2021). Similarly, a wealth of improvements have also been proposed for the solution strategy, including (residual) control algorithms (Ambati et al., 2016; Seleš et al., 2019), quasi-Newton methods (Kristensen and Martínez-Pañeda, 2020; Wu et al., 2020), line search algorithms (Gerasimov and De Lorenzis, 2016; Lampron et al., 2021; Börjesson et al., 2022), and multigrid approaches (Jodlbauer et al., 2020). The computational costs of phase field fracture become particularly demanding when performing cycle-by-cycle computations of fatigue, hindering high cycle fatigue analyses. A common strategy to minimize the costs of computing high cycle fatigue is the use of so-called *cycle jumping*, where the cycle-by-cycle solution is extrapolated to skip the computation of several load cycles (Cojocaru and Karlsson, 2006). Loew et al. (2020) introduced such a scheme for phase field fatigue by locally extrapolating the fatigue history variable.

This paper seeks to introduce alternative means of accelerating cycle-by-cycle phase field fatigue computations. Two methods are proposed which are mutually compatible and individually provide substantial computational performance improvements. Furthermore, neither methods prevent the use of existing cycle jump strategies, which can be included for additional performance improvements. The first computational acceleration method proposed is a modification to existing staggered solution strategies commonly adopted in the phase field literature (Miehe et al., 2010a; Ambati et al., 2014; Seleš et al., 2019), so that the tangent stiffness matrices are not updated in each load step, but rather stored in factorized form such that subsequent increments and iterations are solved with a significant reduced computational cost. This approach, henceforth referred to as *Modified Newton (MN)*, is especially suitable for high-cycle fatigue, where very small changes to the overall system are observed between individual load increments. The second method proposed, referred to as *Constant Load Accumulation (CLA)*, is suitable for problems where only one step of the loading cycle contributes significantly to the fatigue accumulation. For systems where this assumption is valid, the fatigue accumulation rule can be adjusted to permit the simplification of the loading curve to a single load increment per cycle, significantly reducing the total number of increments in the simulation. As shall be shown, for high-cycle problems this approach can be extended to capture multiple load cycles in a single increment with negligible loss of accuracy for even greater computational performance improvement.

The manuscript is organized as follows. Section 2 formulates the phase field fatigue framework used for the cycle-by-cycle computations. The details of the numerical aspects of the finite element solution and the proposed methods are given in Section 3. Subsequently, a series of numerical examples are analyzed in Section 4 to illustrate the capabilities of the proposed method. Concluding remarks end the paper in Section 5.

2. A phase field model for fatigue

This section introduces the specific phase field fatigue model adopted, which is based on the work by Carrara et al. (2020). This choice is grounded on its flexibility, simplicity of implementation and suitability to be used in conjunction with other acceleration schemes (such as those by Loew et al. (2020)). Furthermore, the fatigue acceleration strategies presented here can be readily incorporated into a wide range of phase field fatigue models and, as such, the specific choice phase field model is of secondary importance.

2.1. Basic theory

Consider a solid domain $\Omega \in \mathbb{R}^n$ with boundary $\partial\Omega \in \mathbb{R}^{n-1}$. In a small deformations context, we consider a displacement field $\mathbf{u} \in \mathbb{R}$ and a phase field $\phi \in [0;1]$, for which a value of 0 denotes intact material and a value of 1 denotes broken material with vanishing stiffness. Then, the standard so-called AT2 phase field fracture model (Bourdin et al., 2000) can be formulated from the minimization of the following energy functional:

$$\mathcal{E}(\boldsymbol{\varepsilon}(\mathbf{u}),\phi,\nabla\phi) = \int_\Omega \left[\psi(\boldsymbol{\varepsilon}(\mathbf{u}),\phi) + \frac{G_c}{2}\left(\frac{\phi^2}{\ell} + \ell\nabla\phi\cdot\nabla\phi\right)\right] \mathrm{d}V \tag{1}$$

where G_c is the critical energy release rate or material toughness, ℓ denotes the phase field length scale, and $\psi(\boldsymbol{\varepsilon}(\mathbf{u}),\phi)$ is the strain energy density, which for a linear elastic solid may be expressed as;

$$\psi(\boldsymbol{\varepsilon}(\mathbf{u}),\phi) = (1-\phi)^2\psi_0(\mathbf{u}) = (1-\phi)^2\frac{1}{2}\boldsymbol{\varepsilon}:\mathbf{C}_0:\boldsymbol{\varepsilon}. \tag{2}$$

Here, $\mathbf{C}_0$ is the linear elastic stiffness tensor of the material and $\boldsymbol{\varepsilon}$ is the infinitesimal strain tensor, given by $\boldsymbol{\varepsilon} = (\nabla\mathbf{u} + \nabla\mathbf{u}^T)/2$. The phase field variable, ϕ, is seen to degrade the material stiffness.

2.2. Extension to fatigue

To extend the above fracture framework to account for fatigue damage, Carrara and co-workers (Carrara et al., 2020) proposed introducing a degradation function $f(\bar{\alpha})$, which reduces the material toughness, as a function of an accumulated fatigue history variable $\bar{\alpha}$. Several options are available for both the formulation of the degradation function and the accumulated fatigue history variable. Here, as in Seleš et al. (2021), the accumulated fatigue history variable at time step $n+1$ is introduced as the cumulative positive increments of undegraded elastic strain energy density:

$$\bar{\alpha}_{n+1} = \bar{\alpha}_n + |\psi_{0,n+1} - \psi_{0,n}|H(\psi_{0,n+1} - \psi_{0,n}), \tag{3}$$

where H is the Heaviside function. Also following Carrara et al. (2020), we use the asymptotic fatigue degradation function:

$$f(\bar{\alpha}) = \begin{cases} 0 & \text{if } \bar{\alpha} \le \alpha_T \\ \left(\dfrac{2\alpha_T}{\bar{\alpha}+\alpha_T}\right)^2 & \text{else .} \end{cases} \tag{4}$$

where the threshold parameter α_T introduces a lower limit below which accumulated fatigue does not influence the material toughness. This threshold is here chosen as $\alpha_T = G_c/12\ell$.

2.3. Principle of virtual power

Let us first define the Cauchy stress tensor $\boldsymbol{\sigma}$ in terms of the strain energy density ψ,

$$\boldsymbol{\sigma} = \frac{\partial\psi}{\partial\boldsymbol{\varepsilon}} = (1-\phi)^2\boldsymbol{\sigma}_0 = (1-\phi)^2\mathbf{C}_0:\boldsymbol{\varepsilon}. \tag{5}$$

Then, the internal energy of the system can be expressed as

$$\mathcal{W} = \int_\Omega (1-\phi)^2\boldsymbol{\sigma}_0:\varepsilon\,\mathrm{d}V + \int_\Omega\int_0^t f(\bar{\alpha}(\tau))\frac{G_c}{\ell}\left(\phi\dot{\phi} + \ell^2\nabla\phi\cdot\nabla\dot{\phi}\right)\mathrm{d}\tau\,\mathrm{d}V. \tag{6}$$

Alternatively, the above may be expressed in terms of internal power density as

$$\dot{\mathcal{W}} = \int_\Omega \left[(1-\phi)^2\boldsymbol{\sigma}_0:\dot{\boldsymbol{\varepsilon}} + \frac{\partial\psi}{\partial\phi}\dot{\phi} + f(\bar{\alpha}(t))\frac{G_c}{\ell}\left(\phi\dot{\phi} + \ell^2\nabla\phi\cdot\nabla\dot{\phi}\right)\right]\mathrm{d}V. \tag{7}$$

The external power depends only on the external mechanical loading

$$\dot{\mathcal{F}} = \int_\Omega \mathbf{b}\cdot\dot{\mathbf{u}}\,\mathrm{d}V + \int_{\partial\Omega_t}\mathbf{t}\cdot\dot{\mathbf{u}}\,\mathrm{d}S, \tag{8}$$

where $\partial\Omega_t$ denotes the part of the boundary where mechanical tractions $\mathbf{t}$ are applied and $\mathbf{b}$ are the body forces. Here, the external contributions due to the phase field variable and its work-conjugate are omitted, as

only problems with homogeneous phase field boundary conditions are considered. The balance of virtual power requires

$$\dot{\mathcal{W}} - \dot{\mathcal{F}} = 0, \tag{9}$$

which, after applying integration by parts, may be expressed as:

$$\begin{aligned}&\int_\Omega -\left[(1-\phi)^2\nabla\cdot\boldsymbol{\sigma}_0 + \mathbf{b}\right]\cdot\dot{\mathbf{u}}\,\mathrm{d}V + \int_\Omega \left\{\frac{\partial\psi}{\partial\phi} - \frac{G_c}{\ell}\left[f(\bar{\alpha})\left(\ell^2\nabla^2\phi - \phi\right)\right.\right.\\ &\left.\left. + \ell^2\nabla f(\bar{\alpha})\cdot\nabla\phi\right]\right\}\dot{\phi}\,\mathrm{d}V + G_c\ell\int_{\partial\Omega} f(\bar{\alpha})\nabla\phi\cdot\mathbf{n}\dot{\phi}\,\mathrm{d}S\\ &+ \int_{\partial\Omega_t}\left[(1-\phi)^2\boldsymbol{\sigma}\cdot\mathbf{n} - \mathbf{t}\right]\cdot\dot{\mathbf{u}}\,\mathrm{d}S = 0\end{aligned} \tag{10}$$

The above must hold for arbitrary, kinematically admissible, variations of the velocities $\dot{\mathbf{u}}$ and phase field increments $\dot{\phi}$, which by standard arguments implies the following local balance equations and accompanying boundary conditions:

$$\nabla\cdot\left[(1-\phi)^2\boldsymbol{\sigma}_0\right] + \mathbf{b} = 0 \quad \text{in } \Omega \tag{11}$$

$$-2(1-\phi)\psi_0 + f(\bar{\alpha})\frac{G_c}{\ell}\left(\phi - \ell^2\nabla^2\phi\right) - G_c\ell\nabla f(\bar{\alpha})\cdot\nabla\phi = 0 \quad \text{in } \Omega \tag{12}$$

$$(1-\phi)^2\boldsymbol{\sigma}_0\cdot\mathbf{n} = \mathbf{t} \quad \text{on } \partial\Omega \tag{13}$$

$$\nabla\phi\cdot\mathbf{n} = 0 \quad \text{on } \partial\Omega \tag{14}$$

2.4. Strain energy split to adequately handle compression behaviour

In its original formulation, the phase field fracture model predicts a symmetric behaviour under tension and compression. That is, crack growth is equally driven by compressive and tensile stresses and, since the degradation of the material stiffness is similarly isotropic, the crack faces are allowed to interpenetrate and while carrying no compressive loads. A common strategy to mitigate this is to decompose the strain energy density into active and passive parts such that:

$$\psi = (1-\phi)^2\psi_0^+(\mathbf{u}) + \psi_0^-(\mathbf{u}) \tag{15}$$

where only the active part of the strain energy density (ψ_0^+) contributes to crack growth and only the active part of the stiffness is degraded by the phase field variable. Several suggestions have been made for defining the active and passive parts of the strain energy density, with the two most popular being the volumetric/deviatoric split by Amor et al. (2009) and the spectral split by Miehe et al. (2010b). The volumetric/deviatoric split is given by

$$\begin{aligned}\psi_0^+ &= \frac{1}{2}K\langle\mathrm{tr}\boldsymbol{\varepsilon}\rangle_+^2 + \mu(\boldsymbol{\varepsilon}_{dev}:\boldsymbol{\varepsilon}_{dev})\\ \psi_0^- &= \frac{1}{2}K\langle\mathrm{tr}\boldsymbol{\varepsilon}\rangle_-^2,\end{aligned} \tag{16}$$

where $\langle\,\rangle_\pm$ denotes the two signed Macaulay brackets, $\boldsymbol{\varepsilon}_{dev}$ is the deviatoric part of the strain tensor, K is the bulk modulus and μ is the shear modulus or second Lamé parameter. On the other side, the spectral split is based on a spectral decomposition of the strain tensor: $\boldsymbol{\varepsilon}_\pm = \sum_{a=1}^3\langle\varepsilon_I\rangle_\pm\mathbf{n}_I\otimes\mathbf{n}_I$, where ε_I are the principal strains and $\mathbf{n}_I$ denote the principal strain directions (with $I = 1,2,3$). The, the spectral strain energy decomposition is defined as

$$\psi_0^\pm = \frac{1}{2}\lambda\langle\mathrm{tr}\boldsymbol{\varepsilon}\rangle_\pm^2 + \mu\mathrm{tr}\left(\boldsymbol{\varepsilon}_\pm^2\right), \tag{17}$$

with λ denoting the first Lamé parameter and tr being the trace operator.

A significant improvement to the numerical performance of these splits was introduced with the so-called hybrid scheme by Ambati and co-workers (Ambati et al., 2014), where only the active part of the strain energy contributes to crack growth, but the stiffness is isotropically degraded by damage, with the caveat that degradation only applies if the stress state is predominantly tensile. An alternative strain energy decomposition, which has been shown to be particularly effective for fatigue modelling (Golahmar et al., 2023), is the so-called no-tension split by Freddi and Royer-Carfagni (2010). The no-tension split, first intended for masonry-like materials, filters out contributions from compressive strains more effectively than other approaches. Using λ and μ to denote the Lamé parameters, E and ν respectively being Young's modulus and Poisson's ratio, and taking ε_1, ε_2, ε_3 as the principal strains, with ε_1 being the largest, the strain energy decomposition is given as (Lo et al., 2019) Eq. (18) in Box I.

Unless otherwise stated, this no-tension split by Freddi and Royer-Carfagni (2010) is the one adopted in the numerical experiments reported in this manuscript.

3. Finite element implementation

This section provides details of the numerical implementation of the phase field fatigue model presented in Section 2. The finite element method is used and the solution of the resulting system of equations is discussed, together with the fatigue acceleration methods presented in this work: the Modified Newton (MN) and the Constant Load Accumulation (CLA) solution strategies. The implementation is carried out using the Ferrite.jl finite element library (Carlsson et al., 2021).[1]

3.1. Crack irreversibility

Enforcing damage irreversibility is of critical importance when considering non-monotonic loading. For simplicity, we shall here make use of the so-called history field $\mathcal{H}$ approach pioneered by Miehe et al. (2010a). Accordingly, the history field is defined as the maximum active strain energy density experienced in a point during the loading history

$$\mathcal{H} = \max_{\tau\in[0,t]}\psi_0^+(\tau) \tag{19}$$

and it replaces the active undegraded strain energy density ψ_0^+ as the crack driving force in the phase field equation (12). While this approach is convenient and tends to ease the convergence of the phase field equations, it has also been the target of sensible objections (Linse et al., 2017; Strobl and Seelig, 2020), especially regarding its influence on crack nucleation from non-sharp defects and its non-variational nature. The latter issue is of little relevance here, as the fatigue extension of phase field is not variationally consistent in the form adopted here. A more critical aspect in the case of fatigue is that for variable amplitude loading, only the locally maximal loads will be retained as a crack driving force throughout cycles that also include lower loads. However, this scenario is not relevant to this work, as the numerical examples deal with constant amplitude loading and pre-existing sharp defects.

Another method of enforcing irreversibility of fully formed cracks is the so-called crack-set method by Bourdin et al. (2000), where nodes in which the phase field exceeds a given threshold are added to a set of nodes subject to a $\phi = 1$ Dirichlet condition. Anecdotally, we find that this method seems to ease some convergence issues which have been observed to occur at the original crack tip after some degree of crack growth in high-cycle fatigue simulations, regardless of whether the degraded or undegraded strain energy is used to obtain the fatigue variable. As a result, this work uses both the history variable approach and the crack set method in tandem, with the threshold value for nodes to be added to the crack set chosen as 0.95.

3.2. Solution strategy

The governing Eqs. (11)–(14) can be reformulated in a numerically convenient decoupled form as

$$\begin{aligned}&\int_\Omega\left[(1-\phi)^2\boldsymbol{\sigma}_0 : \delta\boldsymbol{\varepsilon} - \mathbf{b}\cdot\delta\mathbf{u}\right]\mathrm{d}V + \int_{\partial\Omega_t}\mathbf{t}\cdot\delta\mathbf{u}\,\mathrm{d}A = 0\\ &\int_\Omega\left[-2(1-\phi)\psi_0^+\delta\phi + f(\bar{\alpha})G_c\left(\frac{\phi}{\ell}\delta\phi + \ell\nabla\phi\cdot\nabla\delta\phi\right)\right]\mathrm{d}V = 0\end{aligned} \tag{20}$$

[1] The Julia implementation developed is openly shared with the community and made available to download at www.empaneda.com/codes.

$$
\begin{array}{lll}
\text{if} & \varepsilon_3 > 0 & \text{then} \begin{cases} \psi_0^+ = \frac{\lambda}{2}\left(\varepsilon_1+\varepsilon_2+\varepsilon_3\right)^2 + \mu\left(\varepsilon_1^2+\varepsilon_2^2+\varepsilon_3^2\right) \\ \psi_0^- = 0 \end{cases} \\
\text{elseif} & \varepsilon_2 + \nu\varepsilon_3 > 0 & \text{then} \begin{cases} \psi_0^+ = \frac{\lambda}{2}\left(\varepsilon_1+\varepsilon_2+2\nu\varepsilon_3\right)^2 + \mu\left[\left(\varepsilon_1+\nu\varepsilon_3\right)^2+\left(\varepsilon_2+\nu\varepsilon_3\right)^2\right] \\ \psi_0^- = \frac{E}{2}\varepsilon_3^2 \end{cases} \\
\text{elseif} & (1-\nu)\varepsilon_1 + \nu(\varepsilon_2+\varepsilon_3) > 0 & \text{then} \begin{cases} \psi_0^+ = \frac{\lambda}{2}\left[(1-\nu)\varepsilon_1+\nu\varepsilon_2+\nu\varepsilon_3\right]^2 \\ \psi_0^- = \frac{E}{2(1-\nu^2)}\left(\varepsilon_2^2+\varepsilon_3^2+2\nu\varepsilon_2\varepsilon_3\right) \end{cases} \\
 & & \text{else} \begin{cases} \psi_0^+ = 0 \\ \psi_0^- = \frac{\lambda}{2}\left(\varepsilon_1+\varepsilon_2+\varepsilon_3\right)^2 + \mu\left(\varepsilon_1^2+\varepsilon_2^2+\varepsilon_3^2\right) \end{cases}
\end{array}
\tag{18}
$$

Box I.

The weak form Eqs. (20) are then discretized using standard bilinear elements to form the system of equations:

$$
\begin{bmatrix} \mathbf{K}^{\mathbf{uu}} & \mathbf{K}^{\mathbf{u}\phi} \\ \mathbf{K}^{\phi\mathbf{u}} & \mathbf{K}^{\phi\phi} \end{bmatrix} \begin{Bmatrix} \mathbf{u} \\ \boldsymbol{\phi} \end{Bmatrix} = \begin{Bmatrix} \mathbf{r}^{\mathbf{u}} \\ \mathbf{r}^{\phi} \end{Bmatrix} \tag{21}
$$

where $\mathbf{K}$ and $\mathbf{r}$ are stiffness matrices and residuals vectors, respectively. The phase field equations are non-convex with respect to the variables $\mathbf{u}$ and ϕ simultaneously. As a result, the full coupled system is notoriously difficult to solve in a stable and efficient manner (unless unconventional schemes, such as quasi-Newton methods, are used (Kristensen and Martínez-Pañeda, 2020; Wu et al., 2020)). However, the equations are convex with respect to the primary variables individually. Therefore, a common strategy is to solve the system in a decoupled fashion, using alternate minimization. In the following, common staggered schemes are briefly introduced, followed by the proposed modified Newton approach for accelerated fatigue computations.

3.2.1. Standard alternate minimization techniques

Solving the phase field equations by a sequence of alternate minimization of the two decoupled subproblems was popularized by Miehe et al. (2010a). The scheme which was then proposed involves solving each of the subproblems independently until individual convergence is achieved before moving on to the next load increment. This is now commonly referred to as a single-pass scheme and introduces significant sensitivity to the size of the load increments. As was shown by Kristensen and Martínez-Pañeda (2020), this approach may be highly inefficient for fatigue computations. Alternatively, one can use so-called multi-pass schemes where the alternate minimization is repeated until some global convergence criterion is reached. Examples of such convergence criteria can be found in Refs. Ambati et al. (2014) and Seleš et al. (2019). Here, we adopt the same residual-based multi-pass approach as found in Lampron et al. (2021), also adopting the tolerances $\texttt{TOL}_{\texttt{in}} = 10^{-5}$ and $\texttt{TOL}_{\texttt{out}} = 10^{-4}$. The scheme is provided in Algorithm 1 and only differs from the single-pass algorithm by the presence of the `while` loop.

Algorithm 1 Multi-pass alternate minimization

Increment $n+1$
Initialize: $\phi_0 = \phi_n$, $\mathbf{u}_0 = \mathbf{u}_n$, $k = 0$
while $||R_\phi(\mathbf{u}_{k+1}, \phi_{k+1})||_\infty \leq \texttt{TOL}_{\texttt{out}}$ **do**
  Find ϕ_{k+1} such that $||R_\phi\left(\mathbf{u}_k, \phi_{k+1}\right)||_\infty \leq \texttt{TOL}_{\texttt{in}}$
  Find $\mathbf{u}_{k+1}$ such that $||R_{\mathbf{u}}\left(\mathbf{u}_{k+1}, \phi_{k+1}\right)||_\infty \leq \texttt{TOL}_{\texttt{in}}$
  $k \leftarrow 1$
end while
$\phi_{n+1} = \phi_k$, $\mathbf{u}_{n+1} = \mathbf{u}_k$

3.2.2. Modified Newton approach for accelerated fatigue computations

In order to accelerate high cycle fatigue computations, a simple modified Newton approach is introduced. In high cycle fatigue computations, it is generally reasonable to expect that changes to the solution variables will be small between individual load increments. Consequently, changes to the tangent stiffness matrices of the system are also expected to be small. As Newton–Raphson based methods do not require the tangent stiffness matrix to be exact, we here propose to modify the multi-pass staggered algorithm given in Algorithm 1, such that the tangent stiffness is only updated and factorized on an as-needed basis. In this implementation, the tangent stiffness matrices for the two subproblems are updated and factorized if any of the following conditions are met:

- Start of analysis
- One of the subproblems fails to converge in n_i inner Newton iterations.
- A number of load increments n_c have passed without updating the stiffness matrices.

The parameters n_i and n_c may be chosen differently. While we have not attempted a systematic study of optimal values, which will depend on the size of the boundary value problem and the total number of cycles to failure, the results obtained (see Section 4) suggest that choosing n_c to have a higher magnitude in the damage sub-problem will likely result in an improved performance.

3.3. Accelerating calculations by accumulating fatigue damage under a constant load

Another technique for accelerating cycle-by-cycle fatigue computations can be achieved by changing the way in which fatigue is accumulated. Here, henceforth referred to as the Constant Load Accumulation (CLA) acceleration strategy. In the current fatigue model, fatigue is accumulated by positive increments of active strain energy. The load ratio R is here loosely defined in term of applied displacement $\bar{u}$ as

$$
R = \frac{\bar{u}_{min}}{\bar{u}_{max}}. \tag{22}
$$

In the case where $R \geq 0$, the load cycle can be resolved using only two load increments per cycle (loading and unloading). However, only one of these increments actually contributes to fatigue. In the case where $R < 0$, four increments per cycle are required (tensile loading, unloading, compressive loading and unloading). If the compressive loading stage does not contribute significantly to fatigue, only the tensile loading increment is relevant, as illustrated by the dashed blue

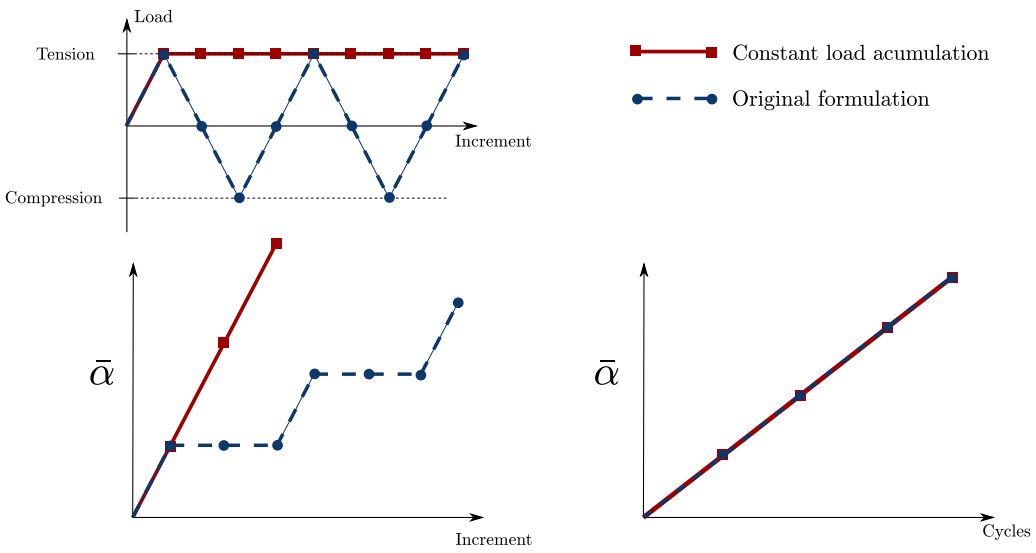

Fig. 1. Illustration of loading pattern and fatigue accumulation for the original formulation on the left and the proposed constant load accumulation scheme of the right. As illustrated, the former requires at least four increments per load cycle, while the latter requires only one.

curves in Fig. 1. Note that these considerations are only intended for high-cycle fatigue where material response is usually well within the linear regime and no effects such as compressive plasticity would be expected to occur to a significant degree. It should also be noted that there are loading conditions where multiple points in the load cycle can be relevant, such as non-proportional loading.

For problems which are sufficiently simple such that only one increment of the load cycle is significant, considerable acceleration of the computation can be achieved by changing the fatigue accumulation from Eq. (3) to

$$\bar{\alpha}_{n+1} = \bar{\alpha}_n + \psi^+_{0,n+1}, \tag{23}$$

and combining this with the application of a constant load $\bar{u} = \bar{u}_{max}$ and the counting of one cycle per increment. The approach is illustrated by solid red lines in Fig. 1. We note for completeness that formally, to account for cases where $R > 0$, the formulation should be amended to

$$\bar{\alpha}_{n+1} = \bar{\alpha}_n + \psi^+_{0,n+1}\left[1 - R^2 H(R)\right], \tag{24}$$

although such cases will not be considered here.

4. Numerical experiments

We shall now present the results of our numerical experiments, aiming at benchmarking the performance of the two novel acceleration strategies proposed here: the Modified Newton (MN) method presented in Section 3.2.2 and the constant load accumulation (CLA) scheme described in Section 3.3. For all the case studies considered, the material parameters are chosen as Young's modulus $E = 210$ GPa, Poisson's ratio $\nu = 0.3$, and toughness $G_c = 2.7\,\mathrm{kJ/m^2}$. First, the growth of fatigue cracks in a Single Edge Notched Tension (SENT) specimen (Section 4.1) is investigated to compare acceleration schemes and quantify gains relative to the reference solution system. Then, more complex cracking patterns are simulated by addressing the nucleation and growth of cracks in an asymmetric three point bending sample containing multiple holes (Section 4.2). Here, one of the objectives is to compare the crack trajectories obtained with different strain energy decomposition approaches. Finally, in Section 4.3, the robustness of the model and its ability to simulate fatigue cracking in large scale 3D problems is demonstrated.

4.1. Fatigue crack growth on a Single Edge Notched Tension (SENT) specimen

The geometry and boundary conditions of the Single Edge Notched Tension (SENT) sample considered in the first case study are shown in Fig. 2(a). The no-tension strain energy density decomposition given in Eq. (18) is used and the initial crack is initialized as a Dirichlet condition on the phase field. The Dirichlet boundary condition is applied on two rows of elements so as to define a constant width for the initial crack.

The specimen is discretized using approximately 32,000 bilinear quadrilateral elements with a refined zone in the crack growth region. In this refined zone, the characteristic element length equals 0.003 mm, more than five times smaller than the phase field length scale, chosen here as $\ell = 0.016$ mm. The specimen is subjected to an alternating applied displacement $\bar{u}$. The fatigue loading is repeated for 120.000 cycles with a maximum applied displacement $\bar{u}_{max} = 0.0002$ mm. Calculations are obtained for four scenarios. First, results are obtained for the standard fatigue accumulation given in Eq. (3) and the multipass staggered algorithm from Algorithm 1. These are considered to be the baseline conditions, not including any of the acceleration strategies proposed in this work. A second scenario constitutes the case where fatigue crack growth is simulated using the Modified Newton (MN) scheme presented in Section 3.2.2. Conversely, the third scenario employs only the Constant Load Acceleration (CLA) scheme described in Section 3.3. Finally, a fourth scenario is considered where both MN and CLA approaches are used in tandem. The MN parameters are chosen as $n_i = 25$ and $n_c = 100$ and the load ratio is always considered to be equal to $R = 0$. All computations are performed with a single core of a CPU of the model Xeon E5-2650 v4.

The finite element predictions of crack extension versus number of cycles are given in Fig. 3. Here, crack extension is measured as the distance between the original crack tip and the furthest point with $\phi = 0.95$. The results reveal that the acceleration schemes do not inherently introduce any deviation in crack extension when compared to the baseline. This is always the case for the modified Newton Method, and holds true for the CLA scheme when there is no compressive contribution to fatigue.

As shown in Table 1, the computational performance of the different modelling strategies is measured by a number of factors. The first measure of performance is the actual computation time (in hours). However, one should note that although noise in this indicator has been

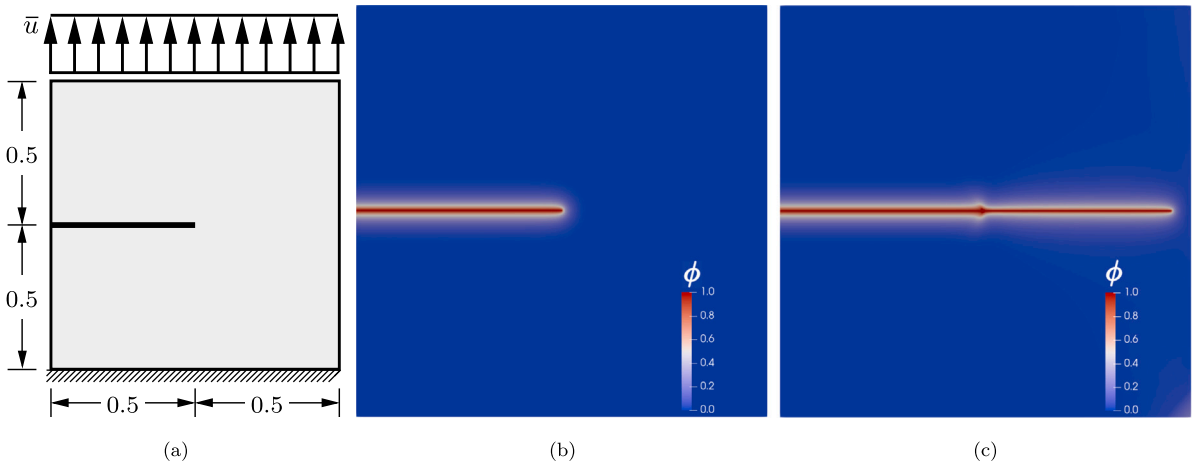

Fig. 2. Fatigue crack growth in a Single Edge Notched Tension (SENT): (a) geometry (with dimensions in mm) and boundary conditions, (b) initial crack contour, and (c) final stage of the fatigue crack propagation.

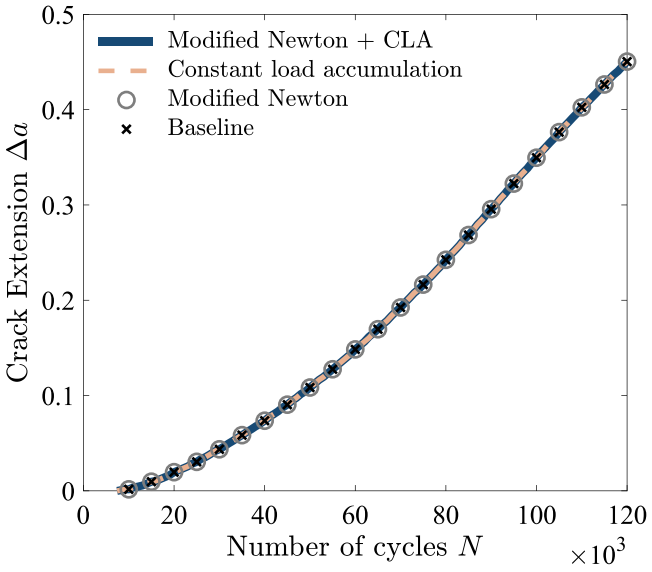

Fig. 3. Predictions of crack extension Δa versus number of cycles N for the SENT case study. The figure shows results obtained with the reference (baseline) conditions, and the two acceleration scheme presented here (Modified Newton, NM; Constant load accumulation, CLA), independently and in tandem.

minimized by the absence of parallel computing and the use of identical CPU types, individual measures of computation time should not be taken as an exact quantification of performance. A more objective measure is the second performance indicator considered, the total number of matrix factorizations, where one factorization here denotes a factorization of both the displacement and the damage subproblems. In addition, Table 1 also provides with the total number of iterations used on the phase field and displacement subproblems. The results reveal that while the use of a constant load accumulation acceleration strategy significantly reduces the computation time by reducing the necessary number of load increments, bringing a similar reduction in iterations and factorizations, the use of the Modified Newton approach presents a trade-off between a reduction in matrix factorizations and an increase in necessary iterations, especially on the displacement problem. However, with the choice of parameters for the modified Newton approach of $n_i = 25$ and $n_c = 100$, this strategy requires roughly 100 times less matrix factorizations than the baseline result in exchange for only 4 times more iterations on the displacement problem. Also, we emphasize

Table 1
Performance details for the SENT case study, comparing baseline results with the use of the Modified Newton (MN) approach, constant load accumulation (CLA) and a combination thereof.

Solutions strategy	MN + CLA	CLA	MN	Baseline
Computation time [h]	13.0	32.7	40.1	96.5
Matrix factorizations	1191	120 032	2379	240 032
Total iterations ϕ	120 205	120 032	240 114	240 032
Total iterations $\mathbf{u}$	276 812	120 032	973 678	240 032

that the iterations on the displacement problem are very cheap when using the MN approach as they only require rebuilding the residuals and trivially finding the solution with the existing factorized stiffness matrix. The results obtained show that both the Modified Newton (MN) and the constant load accumulation (CLA) accumulation strategies can provide substantial performance gains (independently or in tandem) without loss of accuracy. Moreover, these methods are compatible with existing cycle jump schemes such as those presented in Loew et al. (2020) and Seleš et al. (2021).

4.1.1. Additional acceleration with multiple cycles per increment

With the use of the constant load accumulation scheme, the choice of counting one cycle per increment is somewhat arbitrary as the update to the accumulated fatigue variable $\bar{\alpha}$ from increment n to increment $n+1$ can be readily modified to

$$\bar{\alpha}_{n+1} = \bar{\alpha}_n + \mathcal{N}\psi_{0,n+1}, \tag{25}$$

where the number of cycles per increment $\mathcal{N}$ can be chosen smaller or greater than one. While a small degree of error is expected to arise as a result of the discrete sampling of the cycle history that will result from considering $\mathcal{N} > 1$ ("cycle-jumping"), we here show that this error is negligible for simulations involving varying numbers of cycles to failure. To this end, calculations are conducted for the SENT geometry considering three values for the maximum applied displacement, namely $\bar{u}_{max} = 0.00016$ mm, $\bar{u}_{max} = 0.00020$ mm, and $\bar{u}_{max} = 0.00025$ mm, and corresponding characteristic number of cycles equal to 60,000, 120,000 and 240,000, respectively. The number of cycles per increment $\mathcal{N}$ is varied in the range from 1 to 32 to investigate its influence on the accuracy of the solution. In all cases, this enhanced CLA approach is used in conjunction with the Modified Newton method. Results are provided for all three cases in Fig. 4. It can be observed that the accumulated error is small, with deviations in final crack extension from the reference $\mathcal{N} = 1$ being in all cases below 3%. Moreover, for a given value of $\mathcal{N}$, the deviation in the

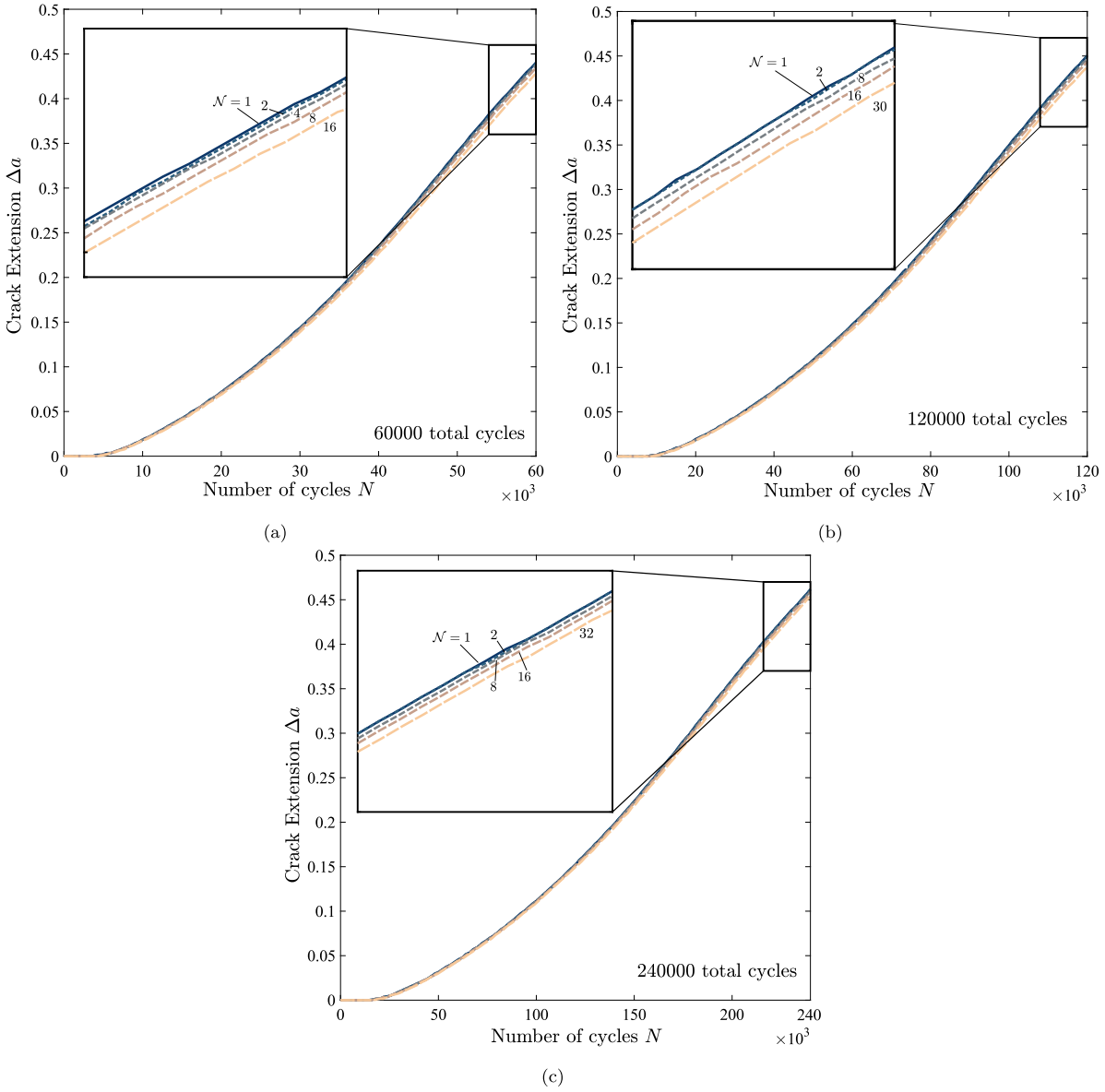

Fig. 4. Predictions of crack extension Δa versus number of cycles N for the SENT case study considering selected values of $\mathcal{N}$ (number of cycles per increment) and the following characteristic number of cycles: (a) 60,000 cycles, (b) 120,000 cycles, and (c) 240,000 cycles.

estimated crack extension at the end of the characteristic number of cycles decreases with increasing characteristic number of cycles. For high-cycle fatigue problems of engineering relevance, where the total number of cycles may be in the order of millions, a high value of $\mathcal{N}$ can be used with insignificant error. Performance tables similar to Table 1 are provided in Appendix. These show that, while computation times do not scale linearly with $\mathcal{N}$, they do monotonically decrease in the range investigated. Relative to the baseline cases in Table 1, the corresponding computation with the Modified Newton method and the constant load accumulation technique with $\mathcal{N} = 16$, is 32 times faster than the baseline case.

4.2. Asymmetric three point bending

The second case study aims at applying the fatigue acceleration schemes to a boundary value problem exhibiting more complex crack growth. As shown in Fig. 5, a plane strain beam containing an array of holes is subjected to three point bending loading conditions. An initial crack is located asymmetric to the loading pins and the holes, inducing mixed-mode cracking. This paradigmatic boundary value problem has been previously investigated in the context of static loading (see, e.g., Refs. Molnár and Gravouil (2017) and Hirshikesh et al. (2019)).

The domain is discretized using roughly 128,000 linear quadrilateral elements, with a characteristic element size $h_e = 0.01$ mm, five times smaller than the phase field length scale. The applied displacement is $\bar{u} = 0.003$ mm, which is cycled for 90,000 load cycles. As is typical for three point bending experiments, the load ratio is assumed to be $R = 0$. Both the modified Newton and the constant load accumulation scheme are exploited to capture the fatigue history in an efficient manner. The computation is carried out using different strain energy density decompositions to the differences in crack trajectory predictions. The obtained crack paths at the end of the analysis are shown in Fig. 6.

We note that in all cases the crack path differs from those observed under monotonic loading; see, e.g., Refs. Molnár and Gravouil (2017) and Mandal et al. (2019). This deviation is explained by the accumulation of fatigue near the holes which leads to the nucleation of new secondary cracks prior to the intersection of the primary crack with the

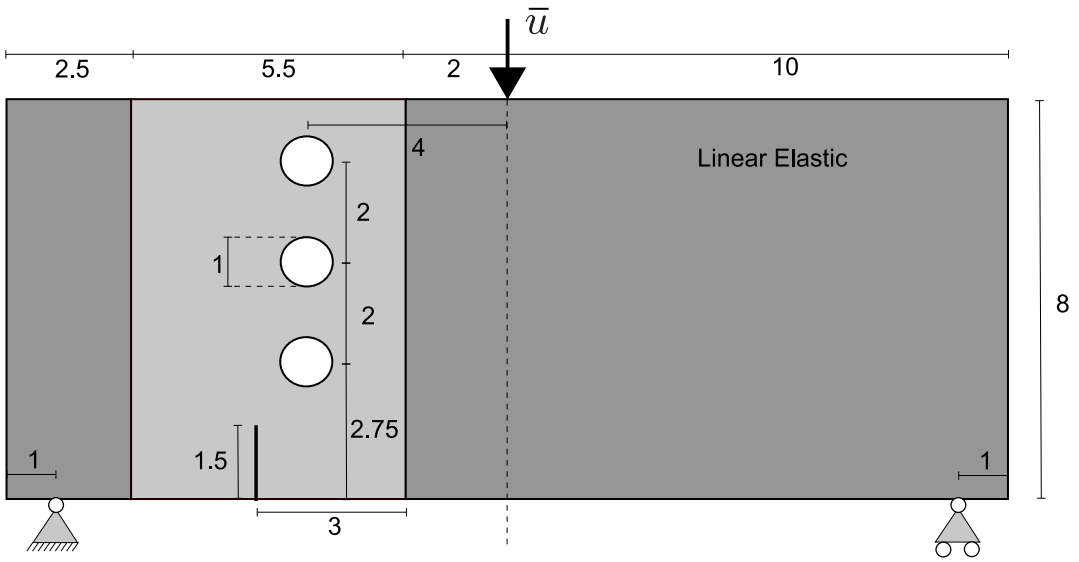

Fig. 5. Sketch of the asymmetric three point bending problem, including dimensions (in mm) and boundary conditions. Only the light grey region is subject to fatigue damage.

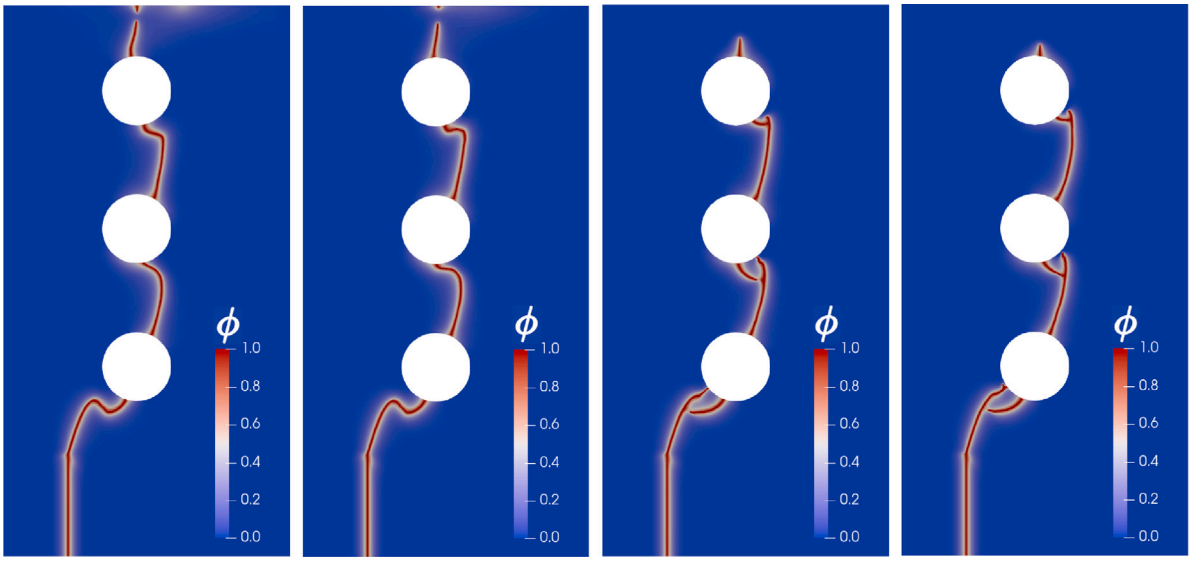

(a) Isotropic (b) Vol/Dev (c) Spectral (d) No-tension

Fig. 6. Asymmetric three point bending: Contours of the phase field crack growth after 90,000 fatigue cycles using (a) no strain decomposition. (b) The volumetric/deviatoric strain decomposition of Amor et al. (2009). (c) The spectral decomposition of Miehe et al. (2010b). (d) The no-tension split of Freddi and Royer-Carfagni (2010).

Table 2
Performance details for the asymmetric three point bending case study as a function of the strain energy decomposition.

Strain decomposition	Isotropic	Volumetric/deviatoric	Spectral	No-tension	No-tension[a]
Computation time [h]	44.9	44.4	60.3	75.5	399.0
Matrix factorizations	1249	1278	1341	1295	180 130
Total iterations ϕ	91 355	91 400	91 742	91 624	180 130
Total iterations **u**	314 292	328 948	400 795	426 645	180 130

[a]Without acceleration schemes.

holes. If an endurance limit were to be introduced in the phase field fatigue formulation, these secondary cracks could be eliminated and the monotonic loading crack path might be recovered. We also remark that the issues with nucleation of cracks from non-sharp defects highlighted by Strobl and Seelig (2020), which stems from the use of the history field approach for crack irreversibility, are not of significance for this phase field fatigue model. Performance measures for the four computations are provided in Table 2.

The spectral and the no-tension split exhibit a more complex crack pattern and also require significantly more iterations on the displacement problem. However, in all cases, the proposed solution strategy offers a large reduction in the number of matrix factorizations required, in exchange for a modest increase in the number of iterations needed on the displacement problem. The results of this case study show that this performance improvement prevails even for complex crack growth studies. In the case of the No-tension split, which took the longest to

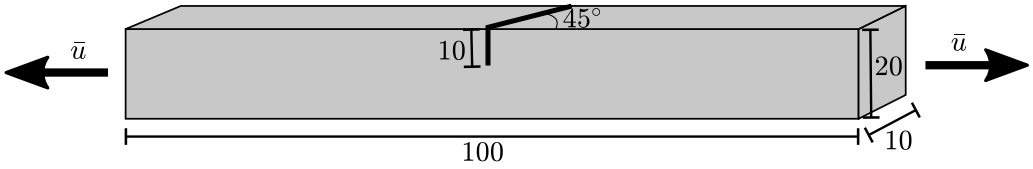

Fig. 7. Sketch of the three-dimensional beam undergoing uniaxial tension and containing a tilted edge crack, including the sample dimensions (in mm) and boundary conditions.

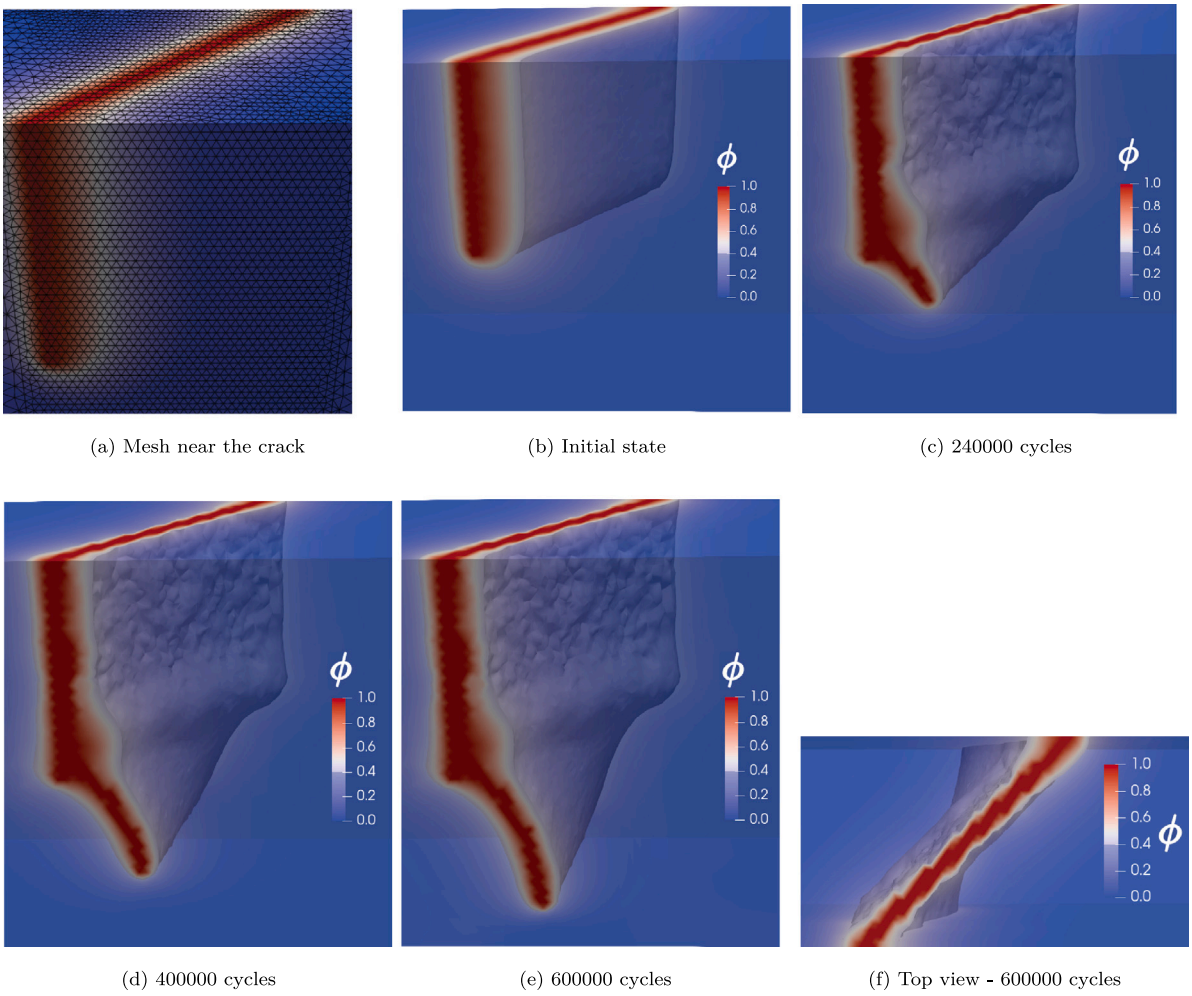

(a) Mesh near the crack (b) Initial state (c) 240000 cycles

(d) 400000 cycles (e) 600000 cycles (f) Top view - 600000 cycles

Fig. 8. Contours of the 3D tension problem. The crack rotates to be perpendicular to the overall maximal principal stress.

compute with the modified Newton approach, it is still more than five times faster than when computed with a standard Newton method and without constant load accumulation. It can be expected that in the absence of these acceleration schemes, computation time is roughly independent of the strain decomposition as only one iteration per field per increment is required even in this most advanced case. Thus, the acceleration is roughly a factor of 9 for the isotropic and volumetric/deviatoric splits. . As it was the case for the SENT specimen, a more optimal performance can most likely be achieved by differentiating how often the stiffness is updated for the two subproblems, as the damage subproblem can be updated far less frequently without paying the price of a significant number of additional iterations.

4.3. 3D beam under tension with a tilted edge crack

As a final benchmark, we consider the uniaxial tension of a three-dimensional beam with an edge crack. The induced complex crack behaviour, the crack is rotated 45° relative to the beam cross section, as sketched in Fig. 7.

The beam is subjected to cyclic tension by means of a displacement boundary condition applied on both ends. The load amplitude is $\bar{u}$ = 1 mm and a total of 600 000 cycles are computed combining the Modified Newton approach with $n_i = 25$ and $n_c = 50$ with the constant load accumulation scheme with $\mathcal{N} = 4$ cycles per increment (see Section 4.1.1). The computational domain is meshed using approximately 196,000 linear tetrahedral elements, with a characteristic length near the crack $h_e = 0.35$ mm. The phase field length scale is here chosen to be equal to $\ell = 1.2$ mm. The results obtained are shown in Fig. 8 in terms of the phase field contours, showing the crack growth pattern.

The results obtained reveal the expected crack growth behaviour, with the crack rotating to position itself perpendicular to the overall maximum principal stress. The proposed methods accelerate the computation significantly, with a total of only 150,000 load increments needed to capture 600,000 cycles during which only 2978 matrix factorizations are performed. In the absence of the Modified

Newton approach and Constant Load Accumulation (CLA) acceleration strategies, a minimum of 1,200,000 increments would be required, with 1,200,000 matrix factorizations and 1,200,000 iterations on each subproblem. Combining the two acceleration schemes proposed here, the computation is achieved using only about 172,000 iterations for the displacement problem and 160,000 for the phase field problem. Furthermore, the majority of these iterations take significantly less time than in the baseline case, as only a few of them require matrix factorization. The number of matrix factorizations, which is the quantity expected to dominate the computation time for large problems, is reduced by a factor of over 400 in total. For a problem with a million cycles, a larger number of cycles per increment $\mathcal{N}$ can be employed for even greater computational improvement without loss of accuracy. Endowed with the acceleration strategies presented in this work, phase field fatigue is shown to be a technologically-relevant tool capable of delivering complex fatigue crack growth predictions in 3D over a hundred thousand cycles.

5. Concluding remarks

We have presented two compelling yet simple methods for accelerating phase field fatigue computations: (i) a Modified Newton (MN) approach, which is shown capable of drastically reducing the number of matrix factorizations necessary in the solution of a high cycle fatigue problem, and (ii) a constant load accumulation (CLA) approach that significantly reduces the number of load increments needed by considering only those relevant to the evolution of the fatigue variable. Three case studies are investigated to explore the performance benefits of these two acceleration strategies, individually and in tandem. Fatigue crack growth is predicted in 2D and 3D scenarios and compared with the baseline model. The results showed that computation times can be reduced by orders of magnitude when using MN and CLA and that these techniques remain robust even in the case of complex crack patterns and three-dimensional crack growth. The acceleration schemes presented enable predicting complex cracking patterns in 3D for over a hundred thousand cycles, endowing phase field fatigue models with the ability of delivering predictions for scales relevant to engineering practice. Moreover, the proposed methods are compatible other accelerations methods such as the cycle jump scheme presented in Loew et al. (2020), which unlocks the potential for even greater performance benefits.

Declaration of competing interest

The authors declare that they have no known competing financial interests or personal relationships that could have appeared to influence the work reported in this paper.

Data availability

Data will be made available on request

Acknowledgements

The authors gratefully acknowledge financial support from the Danish Offshore Technology Centre (DHRTC) under the “Structural Integrity and Lifetime Evaluation” programme as well as. Furthermore, this project would not have been possible without the expertise and resources of the DTU Computing Center (DTU Computing Center, 2021). Emilio Martínez-Pañeda additionally acknowledges financial support from UKRI’s Future Leaders Fellowship programme [grant MR/V024124/1]. A. Golahmar acknowledges financial support from Vattenfall Vindkraft A/S and Innovation Fund Denmark (grant 0153-00018B).

Table 3
Performance details for the SENT specimen at a characteristic number of cycles of 60 000. Computations utilize the proposed modified Newton approach and the constant load accumulation scheme with N cycles per increment.

$\mathcal{N}$	1	2	4	8	16
Computation time [h]	8.7	6.8	4.0	2.2	1.2
Matrix factorizations	606	333	298	294	290
Total iterations ϕ	60 314	30 491	15 600	8131	4528
Total iterations $\mathbf{u}$	234 934	210 754	126 138	71 018	39 680
Crack extension deviation [%]	–	0.19	−0.64	−1.36	−2.9

Table 4
Performance details for the SENT specimen at a characteristic number of cycles of 120,000. Computations utilize the proposed modified Newton approach and the constant load accumulation scheme with N cycles per increment.

$\mathcal{N}$	1	2	8	16	30
Computation time [h]	13.0	9.3	5.3	3.0	1.3
Matrix factorizations	1191	609	293	297	293
Total iterations ϕ	120 205	60 312	15 634	8271	4778
Total iterations $\mathbf{u}$	276 812	227 920	127 541	70 568	40 896
Crack extension deviation [%]	–	0.19	−0.89	−1.51	−2.85

Table 5
Performance details for the SENT specimen at a characteristic number of cycles of 240 000. Computations utilize the proposed modified Newton approach and the constant load accumulation scheme with N cycles per increment.

$\mathcal{N}$	1	2	8	16	32
Computation time [h]	20.6	12.4	7.0	4.0	2.2
Matrix factorizations	2378	1191	320	290	298
Total iterations ϕ	240 150	120 227	30 501	15 614	8186
Total iterations $\mathbf{u}$	357 149	266 701	216 611	127 401	70 764
Crack extension deviation [%]	–	0.00	−0.43	−0.83	−1.74

Appendix. Performance data for the SENT specimen with multiple cycles per increment

We here provide additional performance data for the computations addressed in Section 4.1.1. Specifically, the performance data for the analysis with a characteristic number of cycles equal to 60,000 is given in Table 3, the data pertaining to the analysis for 120,000 cycles is given in Table 4, and the results for the 240,000 cycles case is provided in Table 5. Consistent with the main text, a matrix factorization denotes a factorization of the tangent stiffness matrix of both the damage and the displacement subproblems. The crack extension at the end of the total number of cycles for a given number of cycles per increment $\mathcal{N}$ is denoted a_N. Crack extension deviation is here measure relative to the $\mathcal{N} = 1$ case such that the relative deviation Δa_N is given by:

$$\Delta a_N = \frac{a_N - a_1}{a_1}. \tag{26}$$

References

Ai, W., Wu, B., Martínez-Pañeda, E., 2022. A coupled phase field formulation for modelling fatigue cracking in lithium-ion battery electrode particles. J. Power Sources 544, 231805.

Aldakheel, F., Wriggers, P., Miehe, C., 2018. A modified gurson-type plasticity model at finite strains: formulation, numerical analysis and phase-field coupling. Comput. Mech. 62 (4), 815–833.

Alessi, R., Ambati, M., Gerasimov, T., Vidoli, S., Lorenzis, L.D., 2018. Comparison of phase-field models of fracture coupled with plasticity. Comput. Methods Appl. Sci. 46, 1–21.

Alessi, R., Ulloa, J., 2023. Endowing Griffith’s fracture theory with the ability to describe fatigue cracks. Eng. Fract. Mech. 109048.

Ambati, M., Gerasimov, T., De Lorenzis, L., 2014. A review on phase-field models of brittle fracture and a new fast hybrid formulation. Comput. Mech. 55 (2), 383–405.

Ambati, M., Kruse, R., De Lorenzis, L., 2016. A phase-field model for ductile fracture at finite strains and its experimental verification. Comput. Mech. 57 (1), 149–167.

Amor, H., Marigo, J.J., Maurini, C., 2009. Regularized formulation of the variational brittle fracture with unilateral contact: Numerical experiments. J. Mech. Phys. Solids 57 (8), 1209–1229.

Anand, L., Mao, Y., Talamini, B., 2019. On modeling fracture of ferritic steels due to hydrogen embrittlement. J. Mech. Phys. Solids 122, 280–314.

Borden, M.J., Verhoosel, C.V., Scott, M.A., Hughes, T.J., Landis, C.M., 2012. A phase-field description of dynamic brittle fracture. Comput. Methods Appl. Mech. Engrg. 217–220, 77–95.

Börjesson, E., Remmers, J.J., Fagerström, M., 2022. A generalised path-following solver for robust analysis of material failure. Comput. Mech..

Bourdin, B., Francfort, G.A., Marigo, J.J., 2000. Numerical experiments in revisited brittle fracture. J. Mech. Phys. Solids 48 (4), 1–23.

Bourdin, B., Marigo, J.-J., Maurini, C., Sicsic, P., 2014. Morphogenesis and propagation of complex cracks induced by thermal shocks. Phys. Rev. Lett. 112 (1), 14301.

Boyce, A.M., Martínez-Pañeda, E., Wade, A., Zhang, Y.S., Bailey, J.J., Heenan, T.M., Brett, D.J., Shearing, P.R., 2022. Cracking predictions of lithium-ion battery electrodes by X-ray computed tomography and modelling. J. Power Sources 526, 231119.

Carlsson, K., Ekre, F., Contributors, 2021. Ferrite.jl. URL https://github.com/Ferrite-FEM/Ferrite.jl.

Carrara, P., Ambati, M., Alessi, R., De Lorenzis, L., 2020. A framework to model the fatigue behavior of brittle materials based on a variational phase-field approach. Comput. Methods Appl. Mech. Engrg. 361, 112731.

Cojocaru, D., Karlsson, A.M., 2006. A simple numerical method of cycle jumps for cyclically loaded structures. Int. J. Fatigue 28 (12), 1677–1689.

DTU Computing Center, 2021. DTU Computing Center resources.

Duda, F.P., Ciarbonetti, A., Toro, S., Huespe, A.E., 2018. A phase-field model for solute-assisted brittle fracture in elastic-plastic solids. Int. J. Plast. 102 (November 2017), 16–40.

Feng, Y., Li, J., 2022. Phase-field cohesive fracture theory: A unified framework for dissipative systems based on variational inequality of virtual works. J. Mech. Phys. Solids 159, 104737.

Francfort, G.A., Marigo, J.J., 1998. Revisiting brittle fracture as an energy minimization problem. J. Mech. Phys. Solids 46 (8), 1319–1342.

Freddi, F., Mingazzi, L., 2022. Mesh refinement procedures for the phase field approach to brittle fracture. Comput. Methods Appl. Mech. Engrg. 388, 114214.

Freddi, F., Mingazzi, L., 2023. Adaptive mesh refinement for the phase field method: A FEniCS implementation. Appl. Eng. Sci. 14, 100127.

Freddi, F., Royer-Carfagni, G., 2010. Regularized variational theories of fracture: A unified approach. J. Mech. Phys. Solids 58 (8), 1154–1174.

Gerasimov, T., De Lorenzis, L., 2016. A line search assisted monolithic approach for phase-field computing of brittle fracture. Comput. Methods Appl. Mech. Engrg. 312, 276–303.

Golahmar, A., Kristensen, P.K., Niordson, C.F., Martínez-Pañeda, E., 2022. A phase field model for hydrogen-assisted fatigue. Int. J. Fatigue 154, 106521.

Golahmar, A., Niordson, C.F., Martínez-Pañeda, E., 2023. A phase field model for high-cycle fatigue: Total-life analysis. Int. J. Fatigue 170, 107558.

Guillén-Hernández, T., Quintana-Corominas, A., García, I.G., Reinoso, J., Paggi, M., Turón, A., 2020. In-situ strength effects in long fibre reinforced composites: A micro-mechanical analysis using the phase field approach of fracture. Theor. Appl. Fract. Mech. 108, 102621.

Heister, T., Wheeler, M.F., Wick, T., 2015. A primal-dual active set method and predictor-corrector mesh adaptivity for computing fracture propagation using a phase-field approach. Comput. Methods Appl. Mech. Engrg. 290, 466–495.

Hirshikesh, Natarajan, S., Annabattula, R.K., Martínez-Pañeda, E., 2019. Phase field modelling of crack propagation in functionally graded materials. Composites B 169, 239–248.

Jodlbauer, D., Langer, U., Wick, T., 2020. Matrix-free multigrid solvers for phase-field fracture problems. Comput. Methods Appl. Mech. Engrg. 372, 113431.

Klinsmann, M., Rosato, D., Kamlah, M., McMeeking, R.M., 2015. An assessment of the phase field formulation for crack growth. Comput. Methods Appl. Mech. Engrg. 294, 313–330.

Klinsmann, M., Rosato, D., Kamlah, M., McMeeking, R.M., 2016. Modeling crack growth during Li insertion in storage particles using a fracture phase field approach. J. Mech. Phys. Solids 92, 313–344.

Kristensen, P.K., Martínez-Pañeda, E., 2020. Phase field fracture modelling using quasi-Newton methods and a new adaptive step scheme. Theor. Appl. Fract. Mech. 107, 102446.

Kristensen, P.K., Niordson, C.F., Martínez-Pañeda, E., 2020a. A phase field model for elastic-gradient-plastic solids undergoing hydrogen embrittlement. J. Mech. Phys. Solids 143, 104093.

Kristensen, P.K., Niordson, C.F., Martínez-Pañeda, E., 2020b. Applications of phase field fracture in modelling hydrogen assisted failures. Theor. Appl. Fract. Mech. 110.

Kristensen, P.K., Niordson, C.F., Martínez-Pañeda, E., 2021. An assessment of phase field fracture: Crack initiation and growth. Phil. Trans. R. Soc. A 379 (2203).

Lampron, O., Therriault, D., Lévesque, M., 2021. An efficient and robust monolithic approach to phase-field brittle fracture using a modified Newton method. Comput. Methods Appl. Mech. Engrg. 306.

Linse, T., Hennig, P., Kästner, M., de Borst, R., 2017. A convergence study of phase-field models for brittle fracture. Eng. Fract. Mech. 184, 307–318.

Lo, Y.S., Borden, M.J., Ravi-Chandar, K., Landis, C.M., 2019. A phase-field model for fatigue crack growth. J. Mech. Phys. Solids 132, 103684.

Loew, P.J., Poh, L.H., Peters, B., Beex, L.A., 2020. Accelerating fatigue simulations of a phase-field damage model for rubber. Comput. Methods Appl. Mech. Engrg. 370, 113247.

Lorenzis, L.D., Maurini, C., 2022. Nucleation under multi-axial loading in variational phase-field models of brittle fracture. Int. J. Fract. 237, 61–81.

Mandal, T.K., Nguyen, V.P., Wu, J.Y., 2019. Length scale and mesh bias sensitivity of phase-field models for brittle and cohesive fracture. Eng. Fract. Mech. 217, 106532.

Martínez-Pañeda, E., Golahmar, A., Niordson, C.F., 2018. A phase field formulation for hydrogen assisted cracking. Comput. Methods Appl. Mech. Engrg. 342, 742–761.

Mesgarnejad, A., Imanian, A., Karma, A., 2019. Phase-field models for fatigue crack growth. Theor. Appl. Fract. Mech. 103, 102282.

Miehe, C., Hofacker, M., Welschinger, F., 2010a. A phase field model for rate-independent crack propagation: Robust algorithmic implementation based on operator splits. Comput. Methods Appl. Mech. Engrg. 199 (45–48), 2765–2778.

Miehe, C., Welschinger, F., Hofacker, M., 2010b. Thermodynamically consistent phase-field models of fracture: Variational principles and multi-field FE implementations. Internat. J. Numer. Methods Engrg. 83, 1273–1311.

Molnár, G., Gravouil, A., 2017. 2D and 3D Abaqus implementation of a robust staggered phase-field solution for modeling brittle fracture. Finite Elem. Anal. Des. 130, 27–38.

Navidtehrani, Y., Betegón, C., Martínez-Pañeda, E., 2022. A general framework for decomposing the phase field fracture driving force, particularised to a drucker–prager failure surface. Theor. Appl. Fract. Mech. 121, 103555.

Olesch, D., Kuhn, C., Schlüter, A., Müller, R., 2021. Adaptive numerical integration of exponential finite elements for a phase field fracture model. Comput. Mech. 67 (3), 811–821.

Sargado, J.M., Keilegavlen, E., Berre, I., Nordbotten, J.M., 2021. A combined finite element–finite volume framework for phase-field fracture. Comput. Methods Appl. Mech. Engrg. 373, 113474.

Seiler, M., Linse, T., Hantschke, P., Kästner, M., 2020. An efficient phase-field model for fatigue fracture in ductile materials. Eng. Fract. Mech. 224, 106807.

Seleš, K., Aldakheel, F., Tonković, Z., Sorić, J., Wriggers, P., 2021. A general phase-field model for fatigue failure in brittle and ductile solids. Comput. Mech. 67 (5), 1431–1452.

Seleš, K., Lesičar, T., Tonković, Z., Sorić, J., 2019. A residual control staggered solution scheme for the phase-field modeling of brittle fracture. Eng. Fract. Mech. 205, 370–386.

Simoes, M., Braithwaite, C., Makaya, A., Martínez-Pañeda, E., 2022. Modelling fatigue crack growth in shape memory alloys. Fatigue Fract. Eng. Mater. Struct. 45 (4), 1243–1257.

Simoes, M., Martínez-Pañeda, E., 2021. Phase field modelling of fracture and fatigue in shape memory alloys. Comput. Methods Appl. Mech. Engrg. 373, 113504.

Song, J., Zhao, L.G., Qi, H., Li, S., Shi, D., Huang, J., Su, Y., Zhang, K., 2022. Coupling of phase field and viscoplasticity for modelling cyclic softening and crack growth under fatigue. Eur. J. Mech. A Solids 92, 104472.

Strobl, M., Seelig, T., 2020. Phase field modeling of hertzian indentation fracture. J. Mech. Phys. Solids 143.

Tan, W., Martínez-Pañeda, E., 2021. Phase field predictions of microscopic fracture and R-curve behaviour of fibre-reinforced composites. Compos. Sci. Technol. 202, 108539.

Tanné, E., Li, T., Bourdin, B., Marigo, J.J., Maurini, C., 2018. Crack nucleation in variational phase-field models of brittle fracture. J. Mech. Phys. Solids 110, 80–99.

Wu, J.-Y., 2017. A unified phase-field theory for the mechanics of damage and quasi-brittle failure. J. Mech. Phys. Solids 103, 72–99.

Wu, J.-y.Y., Huang, Y., Phu, V., Nguyen, V.P., 2020. On the BFGS monolithic algorithm for the unified phase field damage theory. Comput. Methods Appl. Mech. Engrg. 360, 112704.

Ye, J.Y., Zhang, L.W., 2022. Damage evolution of polymer-matrix multiphase composites under coupled moisture effects. Comput. Methods Appl. Mech. Engrg. 388, 114213.